



## Article

# Spatial and Temporal Evolution of Precipitation in the Bahr el Ghazal River Basin, Africa

Jinyu Meng<sup>1,2</sup>, Zengchuan Dong<sup>1,\*</sup> , Guobin Fu<sup>2</sup> , Shengnan Zhu<sup>1</sup>, Yiqing Shao<sup>3</sup>, Shujun Wu<sup>1</sup> and Zhuozheng Li<sup>1</sup>

<sup>1</sup> College of Hydrology and Water Resources, Hohai University, Nanjing 210098, China; mengjy@hhu.edu.cn (J.M.)

<sup>2</sup> CSIRO Environment, Wembley, Perth 6913, Australia

<sup>3</sup> Water Conservancy Development Research Center of Taihu Basin Authority Ministry of Water Resource, Shanghai 200434, China

\* Correspondence: zcdong@hhu.edu.cn

**Abstract:** Accurate and punctual precipitation data are fundamental to understanding regional hydrology and are a critical reference point for regional flood control. The aims of this study are to evaluate the performance of three widely used precipitation datasets—CRU TS, ERA5, and NCEP—as potential alternatives for hydrological applications in the Bahr el Ghazal River Basin in South Sudan, Africa. This includes examining the spatial and temporal evolution of regional precipitation using relatively accurate precipitation datasets. The findings indicate that CRU TS is the best precipitation dataset in the Bahr el Ghazal Basin. The spatial and temporal distributions of precipitation from CRU TS reveal that precipitation in the Bahr el Ghazal Basin has a clear wet season, with June–August accounting for half of the annual precipitation and peaking in July and August. The long-term annual total precipitation exhibits a gradual increasing trend from the north to the south, with the southwestern part of the Basin having the largest percentage of wet season precipitation. Notably, the Bahr el Ghazal Basin witnessed a significant precipitation shift in 1967, followed by an increasing trend. Moreover, the spatial and temporal precipitation evolutions reveal an ongoing risk of flooding in the lower part of the Basin; therefore, increased engineering counter-measures might be needed for effective flood prevention.

**Keywords:** remotely sensed precipitation; evaluation; spatial and temporal variability



**Citation:** Meng, J.; Dong, Z.; Fu, G.; Zhu, S.; Shao, Y.; Wu, S.; Li, Z. Spatial and Temporal Evolution of Precipitation in the Bahr el Ghazal River Basin, Africa. *Remote Sens.* **2024**, *16*, 1638. <https://doi.org/10.3390/rs16091638>

Academic Editor: Hatim Sharif

Received: 8 April 2024

Revised: 1 May 2024

Accepted: 2 May 2024

Published: 3 May 2024



**Copyright:** © 2024 by the authors. Licensee MDPI, Basel, Switzerland. This article is an open access article distributed under the terms and conditions of the Creative Commons Attribution (CC BY) license (<https://creativecommons.org/licenses/by/4.0/>).

## 1. Introduction

Precipitation assumes a pivotal role in the intricate dynamics of the near-surface water cycle system, exerting a profound influence on regional water resources [1,2]. A thorough comprehension of the spatial and temporal distribution of precipitation is imperative for diverse applications, spanning flood and drought control, agricultural management, production and livelihood, and ecological monitoring [3–7], among others. Amid the escalating impacts of contemporary climate change, the African continent confronts heightened vulnerability to its adverse effects. Heatwaves, intense rainfall, floods, tropical cyclones, and prolonged droughts exact a devastating toll on Africa’s economic development and the well-being of its inhabitants [8]. Therefore, acquiring precise and timely precipitation information with elevated spatial and temporal resolution in this region is of utmost importance. Reliable precipitation data can effectively underpin flood prediction and control endeavors [9–11]. Nonetheless, the accurate estimation of precipitation remains a formidable challenge due to its discontinuity and high variability in both time and space [12,13].

The principal and most direct modality for quantifying precipitation involves establishing a network of ground-based observations utilizing rain gauges, renowned for their generally precise readings. However, the accuracy of these observations remains

susceptible to diverse natural and perceived factors, encompassing wind, evaporation, human interference, and instrument degradation [14,15]. Moreover, the dearth of efficacious precipitation observation networks in African nations presents a formidable challenge, adding complexity to the acquisition of spatially continuous precipitation information [16].

With advancements in Earth observation, data transmission, and computational technologies, remotely sensed precipitation data have emerged as a pivotal data source for hydrological studies, distinguished by their advantages in expansive coverage and elevated temporal and spatial resolution [17]. This genre of precipitation estimation primarily emanates from the ground-based Global Positioning System (GPS), ground-based weather radar, and satellites. While ground-based radar observation is encumbered by the scarcity of stations and topographical conditions, rendering uniform precipitation observation across extensive areas challenging, the satellite inversion of precipitation adeptly mitigates this constraint. Satellite precipitation inversion relies on various principles, including visible light [18–20], infrared [21,22], microwave [23–25], and a confluence of multiple sensors [26,27]. Through these satellite precipitation inversion algorithms, continuous precipitation data can be derived. This methodology augments the capacity to discern precipitation patterns across a vast geographical expanse, surmounting constraints associated with ground-based observations.

Nonetheless, the precision of satellite precipitation inversion encounters impediments stemming from constraints in physical principles and algorithms, necessitating endeavors to augment accuracy. The amalgamation of precipitation products from diverse data sources emerges as a judicious strategy for refining precision. Consequently, a multi-source precipitation data fusion model is formulated within the theoretical framework of machine learning algorithms and geostatistics, employing auxiliary variables such as topography, latitude, and longitude to enhance the precision of remotely sensed precipitation. Reanalysis data, integrating ground station observations, satellite remote sensing, and numerical model simulations, serve as an amalgamated dataset. Presently, several reanalysis precipitation products find widespread use, encompassing the National Centers for Environmental Prediction's reanalysis (NCEP) in the U.S. [28], the Japan Reanalysis for 55 Years (JRA-55) [29], the U.K.'s National Center for Atmospheric Science Center reanalysis [30], and the European Center for Medium-Range Weather Forecasts reanalysis (ERA-Interim) [31], among others. The incorporation of such reanalysis data further contributes to refining the precision of precipitation estimates through comprehensive data integration.

Reanalysis data, while considered optimal, may not precisely mirror atmospheric conditions, necessitating a thorough comprehension of their performance prior to practical application. Researchers frequently employ rain gauge data from diverse regions to scrutinize the performance of precipitation products and guide their practical implementation. For instance, Jiao et al. [32] assessed the spatial and temporal performance of ERA5 precipitation data from 1979 to 2018, utilizing observations from gridded surface weather stations across China. Their findings indicated that ERA5 adeptly captured interannual and seasonal precipitation patterns, manifesting correlation coefficients ranging from 0.796 to 0.945. However, ERA5 marginally overestimated summer precipitation. The study underscored the impact of topographic distribution and climatic zonation on the accuracy of precipitation products. In a comparative analysis of MERRA, JRA-25, CFSR, and ERA-Interim performance in India, Kishore et al. [33] discerned that ERA-Interim exhibited commendable comparability, followed by CFSR, NASA-MERRA, and JRA-25. Similarly, Huang et al. [34] comprehensively evaluated five reanalysis datasets in reproducing East Asian summer monsoon precipitation, revealing MERRA and ERA-Interim as generally the most reproducible. While the five reanalysis datasets proficiently replicated climatic and interannual variability, they tended to overestimate the frequency of nonrainfall, with JRA-25 and NCEP2 overestimating storm frequency. ERA-Interim and MERRA were lauded for better characterizing interdecadal variability around the mid-1990s. Concerning linear

trends in precipitation, only MERRA reasonably reproduced the trend of escalating precipitation in southern China and the western Pacific, alongside diminishing precipitation in the central and southern peninsulas. Analogous studies evaluating the applicability of MERRA data have been conducted across diverse regions, including Iran, India, Turkey, Australia, and North America [35–41]. Analyzing these studies underscores the variability in the applicability of different datasets across diverse regions.

Nonetheless, extant assessment studies of reanalysis datasets lack sufficient comprehensiveness. The majority of these inquiries concentrate on regions abundant in precipitation data, with fewer assessments undertaken in areas characterized by data scarcity. Paradoxically, these regions already grapple with floods and urgently require substantial precipitation information to effectively address natural disasters such as floods and droughts induced by climate change. Consequently, there exists a compelling need to ascertain the performance of reanalyzed datasets in these critical areas. South Sudan has surfaced as one of the most vulnerable countries globally. United Nations reports underscore that extreme weather events in South Sudan engender natural resource degradation, diminished agricultural yields, food insecurity, and livelihood losses. Climate change has exacerbated weather variability, subjecting the country to heavy rains, seasonal floods, and droughts. Consecutive years of flooding have submerged two-thirds of South Sudan, with the northern city of Bentiu in the Bahr el Ghazal River Basin being the worst affected. This renders the acquisition of high-quality precipitation information pivotal. Hence, this paper focuses on appraising the performance of CRU TS, ERA5, and NCEP data in the Bahr el Ghazal River Basin in Africa. The primary objective is to assess and juxtapose the overall efficacy of CRU TS, ERA5, and NCEP in estimating precipitation across regional and multiple time scales (annual, seasonal, and monthly) and to scrutinize the spatial and temporal trends of precipitation in the Bahr el Ghazal River Basin utilizing the most adept datasets. To the best of our knowledge, this paper constitutes the inaugural study evaluating reanalysis data in the Bahr el Ghazal River Basin, concurrently exploring precipitation trends in the region. This study furnishes invaluable insights for the discerning utilization of reanalyzed precipitation data in the Bahr el Ghazal River Basin, offering pivotal support for flood control in the northern part of South Sudan.

## 2. Materials and Methods

### 2.1. Study Area

The study area encompasses the Bahr el Ghazal River Basin, whose geographical location is illustrated in Figure 1a. The Bahr el Ghazal serves as a tributary to the left bank of the White Nile River, spanning a length of 716 km and embracing a watershed area of 520,000 km<sup>2</sup>. Originating from the northern slopes of the Azande Plateau, the Jur and Tonj Rivers commence their course in southwestern Sudan, meandering northward into Lake Ambadi before assuming the nomenclature Bahr el Ghazal. The river persists in its northeasterly trajectory, merging with the Bahr el-Arab River and ultimately joining the White Nile River, contributing to the replenishment of Lake Noor. Despite the prevalence of rainfall in the Basin, the river imparts a relatively modest water volume to the White Nile, a consequence of significant water losses en route attributed to evaporation and swamp injection.

Figure 1b delineates the climatic types within the Bahr el Ghazal Basin. The northern segment experiences a tropical desert climate with minimal precipitation, giving rise to the Shatt al-Arab River, characterized by a notably low flow rate. The central part manifests a tropical semi-arid climate distinguished by perennially high temperatures and droughts, receiving less than 700 mm of annual rainfall, predominantly during the wet season, with an average daily temperature ranging from 24 to 30 °C. In contrast, the southern part features a savannah climate with an average annual temperature of approximately 25 °C, marked by elevated temperatures throughout the year and distinct dry and wet seasons, with annual precipitation typically ranging from 700 to 1000 mm. In South Sudan, the Bahr el Ghazal Basin predominantly experiences a savannah climate characterized by

high humidity and substantial rainfall. Over the past four years, intensified rainfall has resulted in the inundation of all oil fields and residences located in the lower Bahr el Ghazal region.

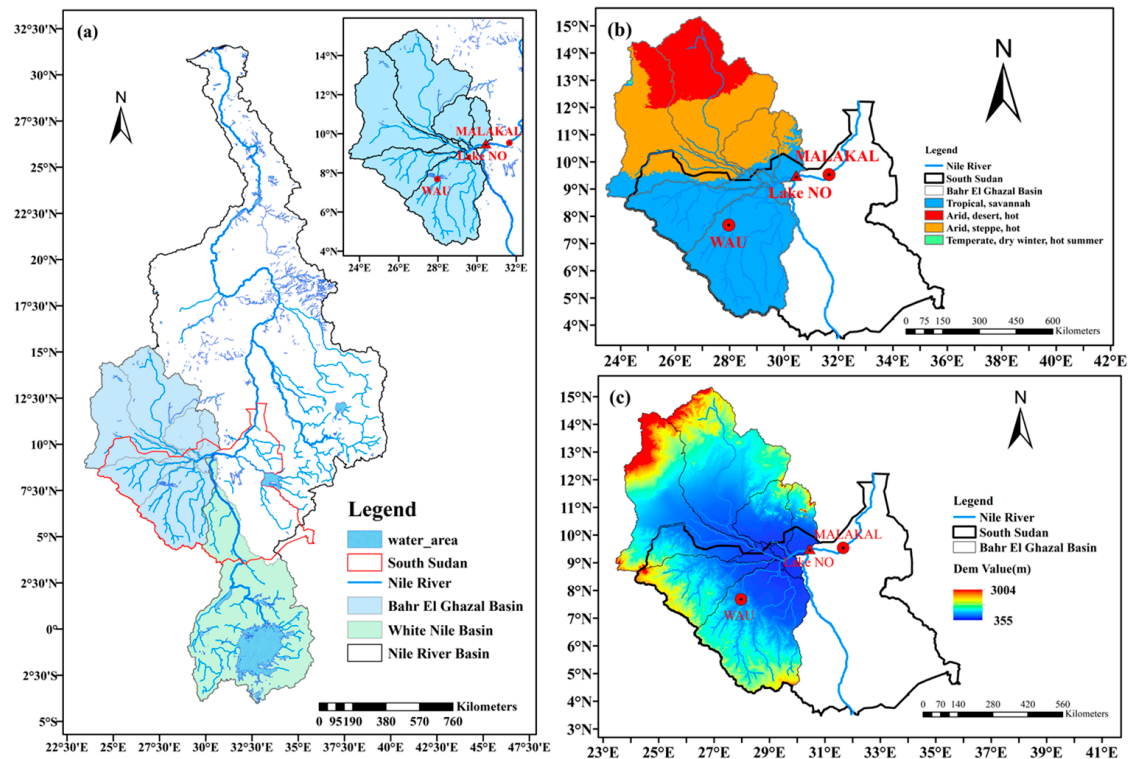


**Figure 1.** (a) Geographic location of the Bahr el Ghazal Basin; (b) spatial distribution of climate types in the Bahr el Ghazal Basin; (c) elevation map of the Bahr el Ghazal Basin.

## 2.2. Datasets

### 2.2.1. Observational Data

The study area pertains to a classification of regions marked by an acute paucity of data, distinguished by a dearth of observational records. The research team acquired the sole accessible measured precipitation data for the cities of WAU and MALAKAL from the Civil Aviation Authority of South Sudan. They were measured by the South Sudan Civil Aviation Authority, but due to the timing of the construction of the airports and a war, this resulted in different periods of data. Precisely, WAU's dataset encompasses monthly precipitation data from 1961 to 2017, while MALAKAL's dataset spans 1961 to 2013, each affording valuable insights into the documented precipitation patterns within these locales.

### 2.2.2. CRU TS

CRU TS stands as one of the most extensively utilized climate datasets, meticulously curated by the National Centre for Atmospheric Science (NCAS) in the United Kingdom. This dataset provides monthly data at a  $0.25^\circ$  resolution, encompassing global land surfaces from 1901 to 2022. The dataset encompasses 10 variables derived from near-surface measurements, including temperature (mean, minimum, maximum, and diurnal temperature range), precipitation (total amount and rainy days), humidity (e.g., vapor pressure), frost days, cloud cover, and potential evapotranspiration. In this study, the CRU TS v4.07 data version was utilized (<https://crudata.uea.ac.uk/cru/data/hrg/> (accessed on 15 September 2022)).

### 2.2.3. ERA5

ERA5 stands as the fifth-generation atmospheric reanalysis dataset of global climate, meticulously crafted by the European Centre for Medium-Range Weather Forecasts (ECMWF), spanning the temporal expanse of January 1950 to the present day. ERA5 boasts a horizontal resolution of  $0.1^\circ \times 0.1^\circ$ . Developed by ECMWF's Copernicus Climate Change Service (C3S), ERA5 furnishes hourly estimates for a spectrum of atmospheric, land, and ocean climate variables. These estimations encapsulate the entire Earth's surface on a 30 km grid, leveraging 137 height levels from the surface up to 80 km to comprehensively capture atmospheric conditions. Uncertainty information for all variables is incorporated when adjusting spatial and temporal resolutions. ERA5 seamlessly integrates model data with global observations, fashioning a dataset that is globally comprehensive and coherent, outperforming its predecessor, the ERA-Interim reanalysis (<https://cds.climate.copernicus.eu/cdsapp#!/dataset/reanalysis-era5-land-monthly-means> (accessed on 15 September 2022)).

### 2.2.4. NCEP

The NCEP/NCAR Reanalysis dataset (referred to as NCEP henceforth) is collaboratively produced by the National Centers for Environmental Prediction (NCEP) and the National Center for Atmospheric Research (NCAR) in the United States. Employing state-of-the-art global data assimilation systems and a comprehensive database, they execute quality control and assimilation processing on observations sourced from various channels, including surface, ships, radiosondes, wind profilers, aircraft, and satellites, among others. This meticulous process yields a comprehensive reanalysis dataset encompassing a diverse array of variables, featuring extensive spatial coverage and extending over a prolonged period (<https://psl.noaa.gov/data/gridded/data.ncep.reanalysis.html> (accessed on 15 September 2022)).

## 2.3. Methods

### 2.3.1. Data Preprocessing

Initially, a preliminary analysis was executed on the two acquired datasets, encompassing the standardization of coordinate systems and time systems.

Subsequently, spatial matching comparisons were performed on the CRU TS, ERA5, and NCEP data. A common method is to compare the grid values with the average of the measurements within the grid [42,43]. However, due to the limited number of actual measurement points (only two) and their considerable distance apart, this study employed interpolation methods for the comparison between grid values and actual measurements.

For spatial interpolation of precipitation, the inverse distance squared weighting method took precedence [44]. In this method, the value at the interpolated location is derived through a weighted average of neighboring points, with the weights determined by a distance function. Common distance metrics include Euclidean distance and Manhattan distance, among others. In this study, the reciprocal of the square of the Euclidean distance was selected as the weighting factor, and the calculation method is as follows:

Calculate the distances between the interpolation point and the four reference points:

$$d_i = \sqrt{(x - x_i)^2 + (y - y_i)^2} \quad (1)$$

Calculate the weights:

$$w_i = \frac{1/d_i^2}{\sum_{i=1}^{i=4} 1/d_i^2} \quad (2)$$

Calculate the value of the interpolation point:

$$P_{(x,y)} = \sum_{i=1}^{i=4} w_i * P(x_i, y_i) \quad (3)$$

where  $x$ ,  $y$  are the coordinates of the interpolated point, and  $x_i, y_i$  are the reference coordinate points.  $P$  is the value of the coordinate point.

### 2.3.2. Evaluation Metrics

We employed the linear correlation coefficient for a comparative analysis of the simulation accuracy of reanalysis data to observational data and utilized relative bias, root mean square error, and mean absolute deviation to assess the level of deviation of reanalysis data from observational data [45,46]. The formula for calculating the correlation coefficient between observed and reanalyzed data for a specific variable is

$$R = \frac{\sum_{i=1}^n (p_i - \bar{p})(o_i - \bar{o})}{\sqrt{\sum_{i=1}^n (p_i - \bar{p})^2 (o_i - \bar{o})^2}} \quad (4)$$

Relative bias is calculated as

$$BIAS = \frac{\sum_{i=1}^n \frac{p_i - o_i}{n}}{\sum_{i=1}^n \frac{o_i}{n}} \times 100 \quad (5)$$

Root Mean Square Error (RMSE) is calculated as

$$RMSE = \sqrt{\frac{\sum_{i=1}^n [(p_i - \bar{p})(o_i - \bar{o})]^2}{n}} \quad (6)$$

Mean Absolute Error (MAE) is calculated as

$$MAE = \sum_{i=1}^n |p_i - o_i| / n \quad (7)$$

where  $n$  is the effective sample size;  $p$  and  $o$  represent reanalysis data and observational data, respectively (mm).

The Taylor diagram succinctly encapsulates the degree of concordance between statistical reanalysis data and observed values. Rooted in the law of cosines, the Taylor diagram delineates three key statistical parameters—correlation coefficient, root mean square error, and standard deviation—on a singular graph. The observed values are positioned as points along the x-axis, one unit away from the origin. The radial length from the origin signifies the variance ratio between reanalysis data and observed values, portraying the likeness in dispersion between reanalysis and observed values. The cosine of the azimuth denotes the correlation coefficient, while the distance from the reanalysis point to the observational point signifies the root mean square error between reanalysis and observation. A shorter distance from the observational point indicates that the reanalysis data are in closer proximity to the observed values.

## 3. Results

### 3.1. Comparative Assessment of the Three Datasets with Observed Data on Time Scales

We assessed the overall performance of CRU TS, ERA5, and NCEP by synthesizing and comparing the congruence of CRU TS, ERA5, and NCEP data with the observed precipitation data of WAU and MALAKAL.

Figure 2 illustrates the total monthly precipitation for WAU and MALAKAL. It is evident that all three datasets proficiently replicate the dry and wet precipitation trends in the study area. CRU TS precipitation exhibits a peak in WAU from January to August and a decline from September to December. It is slightly lower than observed values in MALAKAL from January to June and in November and December, while it is slightly higher than observed values from July to October. ERA5 precipitation is notable during the dry season in WAU and decreases from June to September. Overall, it is larger in the wet season, with the most pronounced increase in October; simulated precipitation exceeds observations in all months of the year at MALAKAL. NCEP shows a smaller

amount than observations in January–March and September–December at WAU and larger amounts than observations in April–August. In MALAKAL, NCEP is smaller than observations from January to June and October to December and larger than observations in July–September. By comparing and analyzing the fitted curves of monthly precipitation for the three datasets with the observations, we can see that the CRU TS precipitation data demonstrate a more realistic representation and superior estimation ability at the monthly scale.

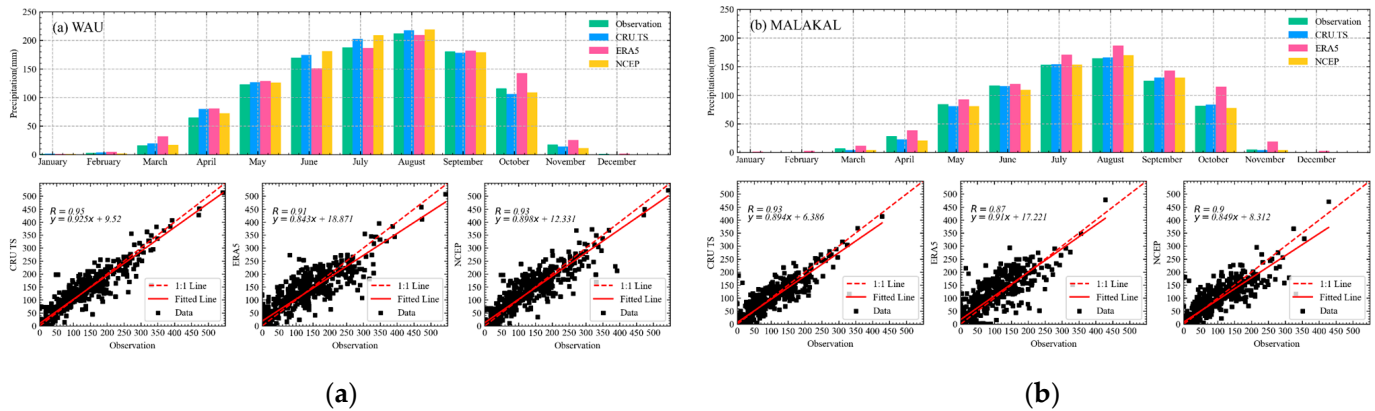


Figure 2. Total monthly precipitation and fitted monthly precipitation. (a) WAU; (b) MALAKAL.

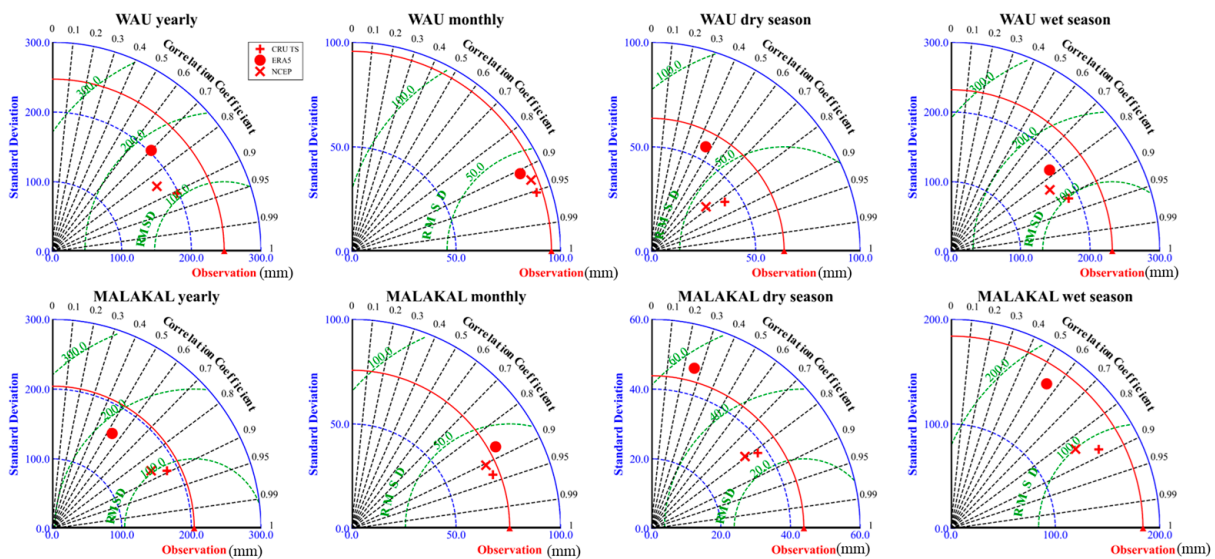
The detailed evaluation results for the three datasets at the two locations are listed in Table 1, and the standard deviation, correlation coefficient, and RMSE are placed in a Taylor diagram (Figure 3) to provide a more intuitive comparison of the three datasets with the observations.

Table 1. Assessment results for the three reanalyzed datasets.

Dataset	Evaluation Metrics	WAU				MALAKAL			
		Monthly	Dry Season	Wet Season	Annual	Monthly	Dry Season	Wet Season	Annual
CRU TS	R	0.953	0.829	0.912	0.907	0.934	0.816	0.882	0.893
	BIAS (%)	3.02	15.86	1.69	3.02	−0.64	−23.08	0.62	−0.64
	RMSE (mm)	29.195	40.399	100.118	112.213	27.033	27.094	86.966	91.853
	MAE (mm)	17.386	31.732	74.047	82.829	15.238	19.271	66.084	71.834
ERA5	R	0.908	0.462	0.772	0.700	0.870	0.260	0.552	0.535
	BIAS (%)	5.07	42.58	1.19	5.07	17.94	88.84	13.95	17.94
	RMSE (mm)	40.369	76.263	148.018	187.398	41.287	66.500	194.838	226.811
	MAE (mm)	26.498	60.216	118.591	149.966	26.452	51.473	164.816	197.543
NCEP	R	0.929	0.775	0.849	0.850	0.904	0.793	0.843	0.864
	BIAS (%)	3.36	1.20	3.59	3.36	−2.10	−28.53	−0.61	−2.10
	RMSE (mm)	35.712	43.099	131.007	139.406	32.411	29.162	99.912	104.840
	MAE (mm)	22.051	34.279	101.780	110.039	18.508	20.378	79.112	82.479

On the monthly scale, both CRU TS and NCEP offer accurate estimates of precipitation for the two locations, with CRU TS demonstrating superiority. On the seasonal scale, only CRU TS performs satisfactorily, with correlation coefficients between simulated and observed values in the dry and wet seasons above 0.8, particularly in the wet season, where the correlation coefficients are around 0.9. In terms of bias, CRU TS shows a bias of 15.86% in precipitation in the dry season of WAU, a bias of 1.69% in the wet season, and a bias of −23.08% in precipitation in the dry season of MALAKAL. The deviation is −23.08% in the dry season and 0.62% in the wet season. A higher deviation in the dry season can be attributed to less precipitation. The deviation also indicates that CRU TS overestimates precipitation in both the dry and wet seasons at

WAU and underestimates it in the dry season while overestimating it in the wet season at MALAKAL.



**Figure 3.** Taylor diagram of precipitation information for three reanalysis datasets.

On the annual scale, again, CRU TS and NCEP exhibit superior modeling capabilities at both locations, with correlation coefficients exceeding 0.8 and relative deviations within  $\pm 3\%$ . The Taylor diagrams underscore that CRU TS has a better estimation ability than ERA5 and NCEP, making it more suitable for the study.

In conclusion, given the availability of only local monthly scale data and only two points of precipitation data, comparisons are limited to the monthly scale and two points. Based on these comparisons, CRU TS is deemed more applicable in WAU and MALAKAL. Consequently, it is extended to the Bahr el Ghazal Basin to study the characteristics of the spatial and temporal distribution of precipitation in the Bahr el Ghazal Basin.

### 3.2. Comparative Assessment of Three Datasets with Observations at Spatial Scales

CRU TS provides precipitation data with a spatial resolution of  $0.25^\circ \times 0.25^\circ$ . In this study, the Kriging interpolation algorithm was utilized to interpolate the spatial resolution to  $0.1^\circ \times 0.1^\circ$ . Figure 4a,b display the spatial distribution of the multi-year average precipitation in the Bahr el Ghazal River Basin from CRU TS for the years 1961–2022 at resolutions of  $0.25^\circ \times 0.25^\circ$  and  $0.1^\circ \times 0.1^\circ$ .

The spatial distribution maps reveal a decrease in precipitation from north to south. The northern region, characterized by a desert climate, experiences multi-year average precipitation of less than 400 mm. The central region, with a tropical monsoon climate, exhibits multi-year average precipitation ranging from 400 to 800 mm. The southern region, featuring a tropical grassland climate, shows precipitation levels between 800 and 1800 mm. Figure 4c,d illustrate the multi-year average precipitation during the dry season and wet season in the Bahr el Ghazal River Basin from CRU TS for the years 1961–2022. A comparison highlights that precipitation is more concentrated during the wet season. In the dry season, precipitation is concentrated in the southern part of the Bahr el Ghazal River Basin, ranging from 100 to 400 mm, while in the wet season, precipitation is concentrated in the southeast, ranging from 900 to 1300 mm.

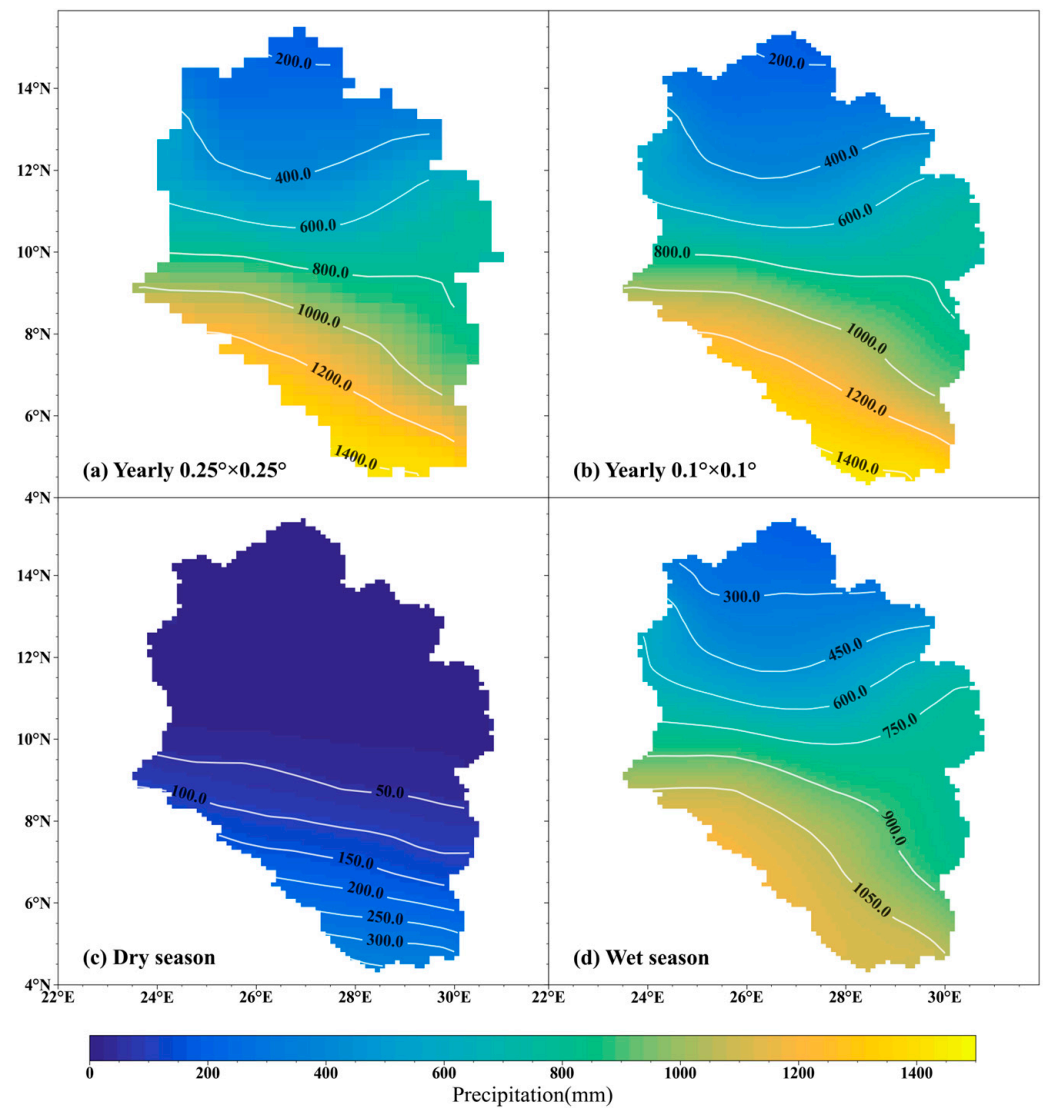


**Figure 4.** Average precipitation in the Bahr el Ghazal River Basin from CRU TS for the years 1961–2022.

Figure 5 illustrates the spatial distribution of monthly average precipitation in the Bahr el Ghazal River Basin from CRU TS for the years 1961–2022. According to the spatial distribution map, during the dry season (November to April of the following year), the northern region of the Bahr el Ghazal River Basin receives almost no precipitation, and even during the rainy season, the monthly average precipitation in the northern region remains within 125 mm. In the central region, there is minimal precipitation during the dry season, and during the rainy season, the monthly average precipitation ranges between 75 and 175 mm. The southern region experiences scarce precipitation during the dry season, averaging around 30 mm, with precipitation concentrating during the rainy season, averaging between 175 and 260 mm. Based on the spatial distribution of precipitation, it can be observed that precipitation follows a three-segment distribution according to climate zones. Therefore, for the analysis of area-averaged precipitation in the Bahr el Ghazal River Basin, the region is divided into three zones—arid desert (AD), tropical monsoon (AS), and tropical savannah (TS)—based on climate distribution. Trend analyses are then conducted for the area-averaged precipitation in each zone.

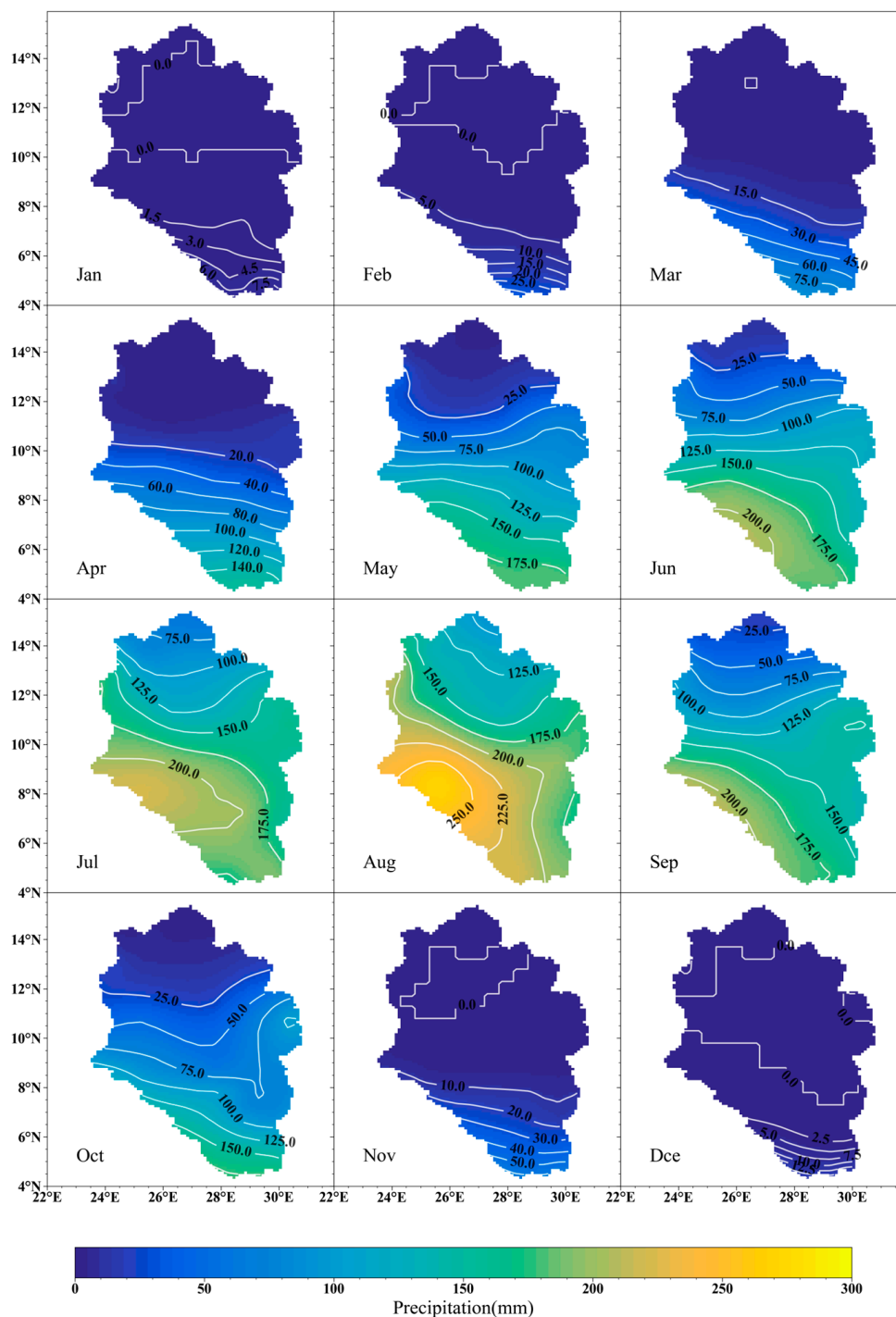
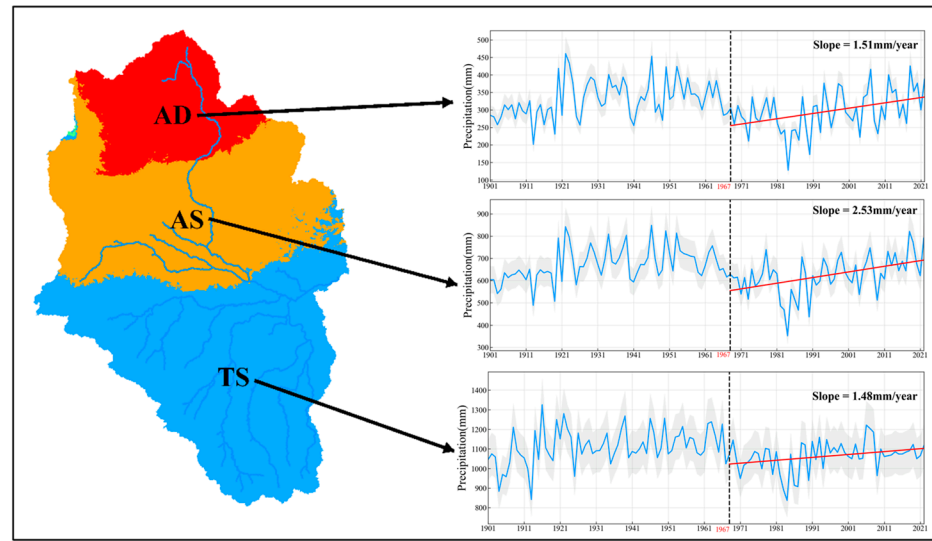


**Figure 5.** Spatial distribution of multi-year monthly average precipitation in the Bahr el Ghazal River Basin from 1961 to 2022 using CRU TS precipitation data.

### 3.3. Bahr el Ghazal River Basin Precipitation Trend Analysis

In this section, the precipitation trends in the Bahr el Ghazal River Basin are analyzed using CRU TS precipitation data. Figure 6 displays the annual precipitation series for different climatic zones in the Bahr el Ghazal River Basin from 1901 to 2022. The precipitation increases gradually from north to south in all three climatic zones, and they exhibit similar trends. Pettitt's test combined with the Mann–Kendall change point test [47,48] is employed to examine the significant change points in the precipitation series for the

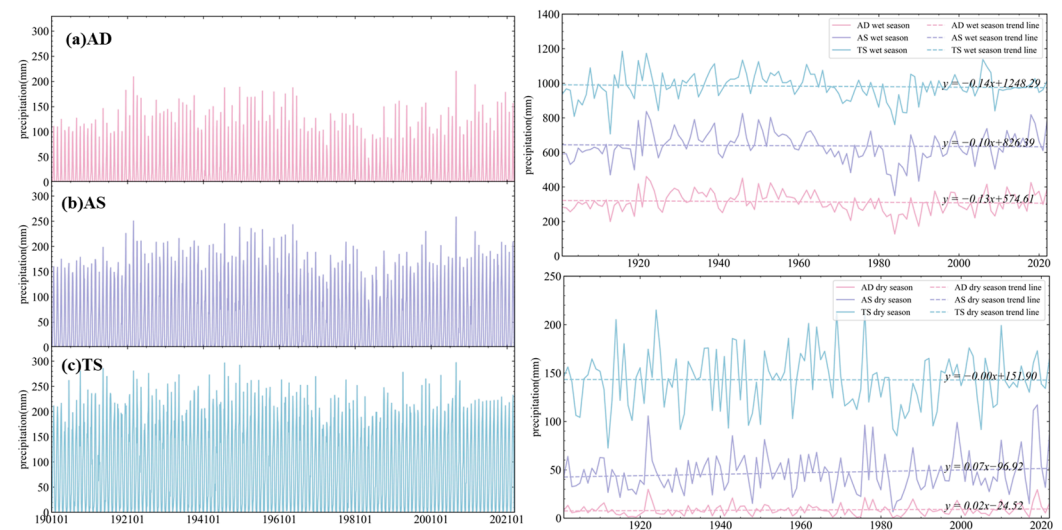
three climatic zones. The results indicate that all three precipitation series experienced a significant ( $\alpha = 0.05$ ) change in 1967.



**Figure 6.** The annual precipitation series for different climatic zones in the Bahr el Ghazal River Basin from 1901 to 2022.

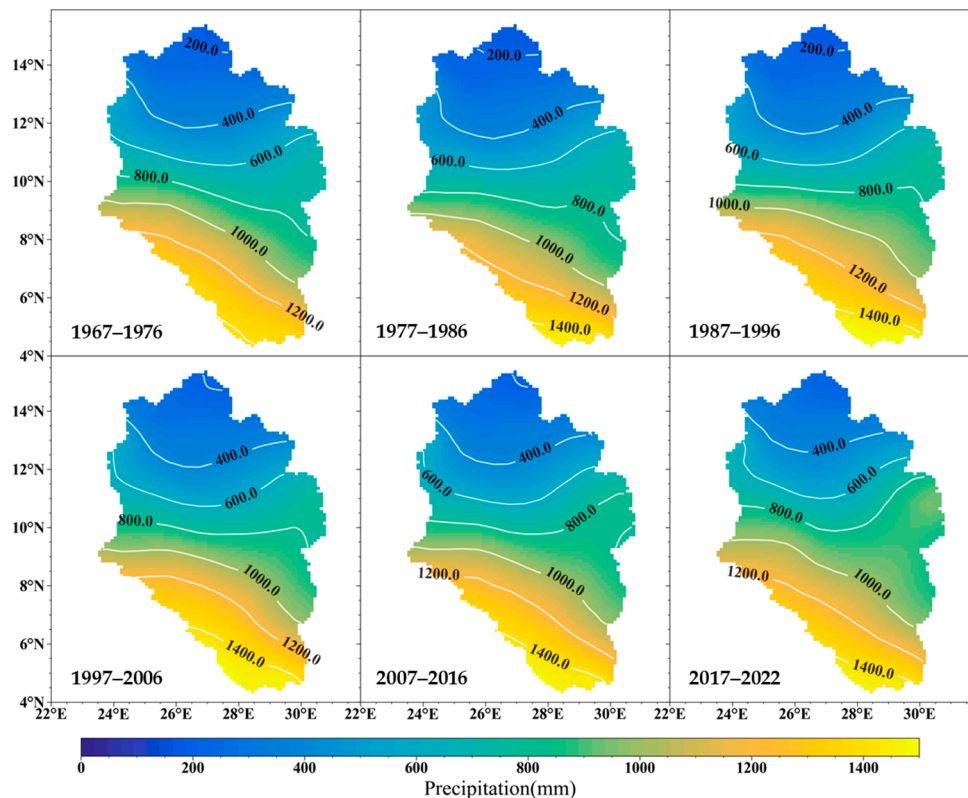
Further trend analyses are conducted using the Cox–Stuart test and the Mann–Kendall test [49–51] for the precipitation series in the three climatic zones from 1967 to 2022. The results reveal a significant ( $\alpha = 0.05$ ) increasing trend in all three precipitation time series, with an annual increase of 1.51 mm in arid desert (AD), 2.53 mm in tropical monsoon (AS), and 1.48 mm in tropical savannah (TS). The climatic zone with a tropical monsoon climate exhibits the most pronounced increase.

Figure 7 shows the monthly and seasonal precipitation processes for the three climate zones, and it is clear from the monthly precipitation processes that the savannah receives more precipitation than the tropical monsoon and the tropical desert. The seasonal precipitation of the three climate zones was then analyzed, and it can be found that, in the dry season, the precipitation of AD and AS showed a non-significant ( $\alpha = 0.05$ ) increasing trend, and the precipitation of the TS region showed no changing trend. In the wet season, all three climatic zones showed a significant ( $\alpha = 0.05$ ) decreasing trend.



**Figure 7.** Monthly and seasonal precipitation processes for three climate zones, 1901–2022.

Figure 8 exhibits the spatial distribution of the decade-average annual precipitation from 1967 to 2022. It can be observed that the 800 mm precipitation line gradually shifts northward, indicating an increase in precipitation in the northern region and a trend toward wetter conditions.



**Figure 8.** Spatial distribution of decade-average precipitation every ten years.

## 4. Discussion

### 4.1. Applicability of Reanalysis Datasets

Accurate precipitation data are essential for understanding spatial and temporal variability and for implementing effective flood control measures. In regions with limited precipitation data, precipitation reanalysis data are extensively utilized. Previous studies have critically examined the performance of diverse datasets in varied geographical contexts. Salvacion et al. [52] noted satisfactory outcomes for both original CRU and downscaled CRU in replicating monthly precipitation patterns in the Philippines. Shi et al. [53] assessed the efficacy of gridded CRU TS precipitation data in elucidating the spatiotemporal characteristics of precipitation in the Three Rivers Source Region (TRHR) from 1961 to 2014. Their findings suggested that CRU TS yielded lower estimates for annual precipitation compared with point rainfall records from 29 meteorological stations but exhibited comparable variability.

Jiang et al. [54] highlighted notable relative biases in ERA5 estimates of precipitation over mainland China compared with satellite precipitation products. Steinkopf et al. [55] conducted a meticulous comparison of ERA5 and ERA-Interim precipitation in Africa, revealing substantial correlations between ERA5, and observed results in interannual variability spatial patterns across all seasons. Zhan et al. [56] evaluated NCEP in sub-Saharan Africa from 1979 to 2012, demonstrating that the reanalysis precipitation dataset could effectively capture the long-term statistical characteristics of drought spatiotemporal patterns.

While these researchers have explored the applicability of CRU TS, ERA5, and NCEP in various regions, our study contributes by comparing their performance in simulating rainfall in the Bahr el Ghazal River Basin in Africa. Given the scarcity of precipitation

data in this region and the occurrence of downstream flooding, simulating precipitation is imperative. Our study, building on prior research, utilizes several statistical indicators to compare the simulation performance of CRU TS, ERA5, and NCEP reanalysis precipitation with limited data from two local stations.

The results indicate that CRU TS demonstrates robust applicability in the Bahr el Ghazal River Basin. For instance, at the WAU station, monthly, wet season, and annual precipitation deviations are approximately 3%, with simulated values slightly exceeding observed values. At the MALAKAL station, monthly, wet season, and annual precipitation deviations are within 1%, with simulated values slightly lower than observed values. A study by Assamnew et al. [57] evaluating the performance of ERA5 in simulating East African rainfall used CRU TS as a reference, signifying its representativeness in East Africa. Akinsanola et al. [58] assessed five different precipitation products for their ability to characterize African rainfall, considering GPCC, CRU, and TRMM the most outstanding datasets suitable for African precipitation assessment.

In summary, our study, alongside prior research, suggests that CRU TS is well suited for simulating precipitation in the Bahr el Ghazal River Basin.

#### *4.2. Characterization of the Spatial and Temporal Evolution of Precipitation in the Bahr el Ghazal Basin*

Research on precipitation in the Bahr el Ghazal River Basin is limited, yet precipitation data for this Basin hold significant ( $\alpha = 0.05$ ) importance for flood control, drainage, and secure oil field operations in South Sudan. In the current context of African precipitation research, Ongoma et al. [59] analyzed the spatiotemporal variability of East African precipitation from 1951 to 2010 using the Climate Research Unit (CRU) monthly rainfall and Global Precipitation Climatology Centre (GPCC) rainfall datasets. They found both decreasing and increasing trends, with substantial declines in rainfall from March to May. The 1960s showed the highest annual rainfall change rate, reaching  $-21.76$  mm/year. Omoj et al. [60] studied the distribution of precipitation in South Sudan using data from five stations, including WAU, MALAKAL, and JUBA. Their findings indicated that South Sudan's rainfall is unimodal, with peaks in July and August. June to August (JJA) constitutes the main rainy season, contributing over 50% of annual rainfall. This aligns with our study's results, where Bahr el Ghazal River Basin precipitation primarily concentrates in the wet season from May to October, with the highest peak in July and August. Precipitation from June to August accounts for half of the annual precipitation.

In our study, the Bahr el Ghazal River Basin was divided into three regions based on climatic differences: tropical desert (AD), tropical monsoon (AS), and tropical savannah (TS). We analyzed their temporal trends and found that, after a breakpoint in 1967, all regions exhibited an increasing trend. The Tropical Monsoon region showed the most pronounced growth at 2.53 mm/year. Hamadalnel et al. [61] assessed the historical trend of Sudan's monthly rainfall from 1960 to 2019 using data from 22 locations. The results showed a growth rate of 0.0403 mm/season during 1990–2019. Since the northern part of the Bahr el Ghazal River is located in Sudan, the results of Hamadalnel et al. [61] are somewhat relevant to our study, confirming an increasing trend. In terms of spatial change trends, the northward shift of the 800 mm precipitation line indicates a moistening trend in the northern region. In the context of global climate change, increased extreme weather events alter climate characteristics in some regions. Our study suggests that the impact of climate change on the Bahr el Ghazal River Basin manifests in increased precipitation in the tropical monsoon region.

## **5. Conclusions**

Precipitation stands as a fundamental facet of the hydrological cycle, and alterations in precipitation patterns wield a profound influence on the distribution of surface water. Consequently, obtaining precise and timely information regarding precipitation is imperative for comprehending hydrological processes and averting water-related calamities.

In data-scarce regions like the Bahr el Ghazal River Basin in Africa, fine spatiotemporal resolution and enhanced reanalysis data via numerical simulations emerge as indispensable tools for deciphering local precipitation patterns. Thus, the evaluation of the applicability of reanalysis data in the Bahr el Ghazal River Basin assumes paramount importance.

This study meticulously scrutinized the performance of the CRU TS, ERA5, and NCEP reanalysis datasets, leveraging observed precipitation data from WAU and MALAKAL. The assessment unfolded across four evaluation metrics and various temporal scales encompassing monthly, seasonal, and annual dimensions. Additionally, an in-depth analysis of the spatiotemporal distribution characteristics of precipitation in the Bahr el Ghazal River Basin was conducted, leading to the following conclusions:

1. Comparative analysis unveiled that the CRU TS dataset excels in simulating precipitation characteristics in the Bahr el Ghazal River Basin, particularly at monthly, seasonal, and annual scales.
2. Temporal distribution analysis of precipitation in the Bahr el Ghazal River Basin highlighted a concentration during the wet season from May to October, with the zenith of precipitation occurring in July and August. Contributions to annual precipitation are notably prominent from June to August.
3. Spatial distribution analysis delineated spatial variability in precipitation across the Bahr el Ghazal River Basin. During the dry season, precipitation is virtually absent throughout the entire Basin. In the wet season, precipitation gradually intensifies from north to south, with scarcity in the northern region and concentration in the southwestern part of the Basin.
4. Based on climate zones, the Bahr el Ghazal River Basin was stratified into three regions. Each of these regions experienced a significant breakpoint in precipitation in 1967, followed by a discernible upward trajectory in precipitation from 1967 to 2022.
5. Spatial trend analysis showcased a northward shift in the 800 mm precipitation line, signifying a moistening trend in the northern part of the Bahr el Ghazal River Basin.

In summation, CRU TS exhibits commendable applicability for simulating precipitation in the Bahr el Ghazal River Basin, rendering it well suited for unraveling the spatiotemporal distribution of precipitation. Nevertheless, it is worth acknowledging that other datasets not included in this comparative analysis may potentially offer more nuanced depictions of precipitation in the Bahr el Ghazal River Basin. To the best of our knowledge, this study stands as the inaugural endeavor to compare the applicability of reanalysis precipitation data in the Bahr el Ghazal River Basin and scrutinize its spatiotemporal distribution. It adeptly addresses a research void in precipitation studies within the Bahr el Ghazal River Basin, supplying invaluable guidance for flood control initiatives in the region and providing pertinent references for downstream South Sudan in the realms of flood prevention, drainage, and efficient oilfield exploitation.

**Author Contributions:** Conceptualization, Z.D.; methodology, J.M.; software, S.Z.; validation, Z.L.; data curation, Y.S.; writing—original draft preparation, J.M.; writing—review and editing, G.F.; visualization, S.W. All authors have read and agreed to the published version of the manuscript.

**Funding:** The work is financially supported by State Grid Corporation Northwest Branch Hydrometeorological Intelligence Project (SGTYHT/21-JS-226), the Postgraduate Research & Practice Innovation Program of Jiangsu Province (KYCX23 0714) and the China Scholarship Council (202306710096).

**Data Availability Statement:** The dataset is available upon request from the authors.

**Acknowledgments:** We thank the South Sudan Civil Aviation Authority for providing precipitation data. We would also like to thank the three anonymous reviewers for their invaluable comments and constructive suggestions used to improve the quality of the manuscript.

**Conflicts of Interest:** The authors declare no conflicts of interest.

## References

1. Foufoula-Georgiou, E.; Guilloteau, C.; Nguyen, P.; Aghakouchak, A.; Hsu, K.-L.; Busalacchi, A.; Turk, F.J.; Peters-Lidard, C.; Oki, T.; Duan, Q.; et al. Advancing precipitation estimation, prediction, and impact studies. *Bull. Am. Meteorol. Soc.* **2020**, *101*, E1584–E1592. [[CrossRef](#)] [[PubMed](#)]
2. Kucera, P.A.; Ebert, E.E.; Turk, F.J.; Levizzani, V.; Kirschbaum, D.; Tapiador, F.J.; Loew, A.; Borsche, M. Precipitation from space: Advancing Earth system science. *Bull. Am. Meteorol. Soc.* **2013**, *94*, 365–375. [[CrossRef](#)]
3. Stephens, E.; Day, J.J.; Pappenberger, F.; Cloke, H. Precipitation and floodiness. *Geophys. Res. Lett.* **2015**, *42*, 10,316–10,323. [[CrossRef](#)]
4. Fowler, H.J.; Wilby, R.L. Detecting changes in seasonal precipitation extremes using regional climate model projections: Implications for managing fluvial flood risk. *Water Resour. Res.* **2010**, *46*. [[CrossRef](#)]
5. Hatfield, J.L.; Boote, K.J.; Kimball, B.A.; Ziska, L.H.; Izaurrealde, R.C.; Ort, D.; Thomson, A.M.; Wolfe, D. Climate impacts on agriculture: Implications for crop production. *Agron. J.* **2011**, *103*, 351–370. [[CrossRef](#)]
6. Rojas, M.; Lambert, F.; Ramirez-Villegas, J.; Challinor, A.J. Emergence of robust precipitation changes across crop production areas in the 21st century. *Proc. Natl. Acad. Sci. USA* **2019**, *116*, 6673–6678. [[CrossRef](#)]
7. Manel, S.; Gugerli, F.; Thuiller, W.; Alvarez, N.; Legendre, P.; Holderegger, R.; Gielly, L.; Taberlet, P.; IntraBioDiv Consortium. Broad-scale adaptive genetic variation in alpine plants is driven by temperature and precipitation. *Mol. Ecol.* **2012**, *21*, 3729–3738. [[CrossRef](#)] [[PubMed](#)]
8. Connolly-Boutin, L.; Smit, B. Climate change, food security, and livelihoods in sub-Saharan Africa. *Reg. Environ. Chang.* **2016**, *16*, 385–399. [[CrossRef](#)]
9. Tarek, M.; Brisette, F.P.; Arsenaault, R. Evaluation of the ERA5 reanalysis as a potential reference dataset for hydrological modelling over North America. *Hydrol. Earth Syst. Sci.* **2020**, *24*, 2527–2544. [[CrossRef](#)]
10. Ababaei, B. Spatio-temporal variations of seven weather variables in Iran: Application of CRU TS and GPCC data sets. *Irrig. Drain.* **2020**, *69*, 164–185. [[CrossRef](#)]
11. Saha, S.; Moorthi, S.; Pan, H.L.; Wu, X.; Wang, J.; Nadiga, S.; Tripp, P.; Kistler, R.; Woollen, J.; Behringer, D.; et al. NCEP climate forecast system reanalysis (CFSR) monthly products, January 1979 to December 2010. *Bull. Amer. Meteor. Soc.* **2010**, *91*, 1015–1057. [[CrossRef](#)]
12. Stephens, G.L.; L'Ecuyer, T.; Forbes, R.; Gettelmen, A.; Golaz, J.; Bodas-Salcedo, A.; Suzuki, K.; Gabriel, P.; Haynes, J. Dreary state of precipitation in global models. *J. Geophys. Res. Atmos.* **2010**, *115*. [[CrossRef](#)]
13. Donat, M.G.; Lowry, A.L.; Alexander, L.V.; O'Gorman, P.A.; Maher, N. More extreme precipitation in the world's dry and wet regions. *Nat. Clim. Chang.* **2016**, *6*, 508–513. [[CrossRef](#)]
14. Fallah, A.; Rakhshandehroo, G.R.; Berg, P.; O, S.; Orth, R. Evaluation of precipitation datasets against local observations in southwestern Iran. *Int. J. Climatol.* **2020**, *40*, 4102–4116. [[CrossRef](#)]
15. Haiden, T.; Kann, A.; Wittmann, C.; Pistotnik, G.; Bica, B.; Gruber, C. The Integrated Nowcasting through Comprehensive Analysis (INCA) system and its validation over the Eastern Alpine region. *Weather Forecast.* **2011**, *26*, 166–183. [[CrossRef](#)]
16. Roffe, S.J.; van der Walt, A.J. Representation and evaluation of southern Africa's seasonal mean and extreme temperatures in the ERA5-based reanalysis products. *Atmos. Res.* **2023**, *284*, 106591. [[CrossRef](#)]
17. Sultana, R.; Nasrollahi, N. Evaluation of remote sensing precipitation estimates over Saudi Arabia. *J. Arid Environ.* **2018**, *151*, 90–103. [[CrossRef](#)]
18. Sorooshian, S.; AghaKouchak, A.; Arkin, P.; Eylander, J.; Foufoula-Georgiou, E.; Harmon, R.; Hendrickx, J.M.; Imam, B.; Kuligowski, R.; Skahill, B.; et al. Advanced concepts on remote sensing of precipitation at multiple scales. *Bull. Am. Meteorol. Soc.* **2011**, *92*, 1353–1357. [[CrossRef](#)]
19. Arkin, P.A.; Meisner, B.N. The relationship between large-scale convective rainfall and cold cloud over the western hemisphere during 1982–84. *Mon. Weather Rev.* **1987**, *115*, 51–74. [[CrossRef](#)]
20. Ba, M.B.; Gruber, A. GOES multispectral rainfall algorithm (GMSRA). *J. Appl. Meteorol. Climatol.* **2001**, *40*, 1500–1514. [[CrossRef](#)]
21. Griffith, C.G.; Woodley, W.L.; Grube, P.G.; Martin, D.W.; Stout, J.; Sikdar, D.N. Rain estimation from geosynchronous satellite imagery—Visible and infrared studies. *Mon. Weather Rev.* **1978**, *106*, 1153–1171. [[CrossRef](#)]
22. Xie, P.; Arkin, P.A. Global precipitation: A 17-year monthly analysis based on gauge observations, satellite estimates, and numerical model outputs. *Bull. Am. Meteorol. Soc.* **1997**, *78*, 2539–2558. [[CrossRef](#)]
23. Liu, G.; Curry, J.A. Retrieval of precipitation from satellite microwave measurement using both emission and scattering. *J. Geophys. Res. Atmos.* **1992**, *97*, 9959–9974. [[CrossRef](#)]
24. Weng, F.; Zhao, L.; Ferraro, R.R.; Poe, G.; Li, X.; Grody, N.C. Advanced microwave sounding unit cloud and precipitation algorithms. *Radio Sci.* **2003**, *38*, 33-1–33-3. [[CrossRef](#)]
25. Iguchi, T.; Kozu, T.; Meneghini, R.; Awaka, J.; Okamoto, K.I. Rain-profiling algorithm for the TRMM precipitation radar. *J. Appl. Meteorol. Climatol.* **2000**, *39*, 2038–2052. [[CrossRef](#)]
26. Huffman, G.J.; Bolvin, D.T.; Nelkin, E.J.; Wolff, D.B.; Adler, R.F.; Gu, G.; Hong, Y.; Bowman, K.P.; Stocker, E.F. The TRMM multisatellite precipitation analysis (TMPA): Quasi-global, multiyear, combined-sensor precipitation estimates at fine scales. *J. Hydrometeorol.* **2007**, *8*, 38–55. [[CrossRef](#)]
27. Joyce, R.J.; Janowiak, J.E.; Arkin, P.A.; Xie, P. CMORPH: A method that produces global precipitation estimates from passive microwave and infrared data at high spatial and temporal resolution. *J. Hydrometeorol.* **2004**, *5*, 487–503. [[CrossRef](#)]

28. Kalnay, E.; Kanamitsu, M.; Kistler, R.; Collins, W.; Deaven, D.; Gandin, L.; Iredell, M.; Saha, S.; White, G.; Woollen, J.; et al. The NCEP/NCAR 40-year reanalysis project. In *Renewable Energy*; Routledge: London, UK, 2011; pp. Vol1\_146–Vol1\_194.
29. Kobayashi, S.; Ota, Y.; Harada, Y.; Ebata, A.; Moriya, M.; Onoda, H.; Onogi, K.; Kamahori, H.; Kobayashi, C.; Endo, H.; et al. The JRA-55 reanalysis: General specifications and basic characteristics. *J. Meteorol. Soc. Jpn. Ser. II* **2015**, *93*, 5–48. [[CrossRef](#)]
30. Harris, I.; Osborn, T.J.; Jones, P.; Lister, D. Version 4 of the CRU TS monthly high-resolution gridded multivariate climate dataset. *Sci. Data* **2020**, *7*, 109. [[CrossRef](#)]
31. Balsamo, G.; Albergel, C.; Beljaars, A.; Boussetta, S.; Brun, E.; Cloke, H.; Dee, D.; Dutra, E.; Muñoz-Sabater, J.; Pappenberger, F.; et al. ERA-Interim/Land: A global land surface reanalysis data set. *Hydrol. Earth Syst. Sci.* **2015**, *19*, 389–407. [[CrossRef](#)]
32. Jiao, D.; Xu, N.; Yang, F.; Xu, K. Evaluation of spatial-temporal variation performance of ERA5 precipitation data in China. *Sci. Rep.* **2021**, *11*, 17956. [[CrossRef](#)]
33. Kishore, P.; Jyothi, S.; Basha, G.; Rao, S.V.B.; Rajeevan, M.; Velicogna, I.; Sutterley, T.C. Precipitation climatology over India: Validation with observations and reanalysis datasets and spatial trends. *Clim. Dyn.* **2016**, *46*, 541–556. [[CrossRef](#)]
34. Huang, D.Q.; Zhu, J.; Zhang, Y.C.; Huang, Y.; Kuang, X.Y. Assessment of summer monsoon precipitation derived from five reanalysis datasets over East Asia. *Q. J. R. Meteorol. Soc.* **2016**, *142*, 108–119. [[CrossRef](#)]
35. Duethmann, D.; Zimmer, J.; Gafurov, A.; Güntner, A.; Kriegel, D.; Merz, B.; Vorogushyn, S. Evaluation of areal precipitation estimates based on downscaled reanalysis and station data by hydrological modelling. *Hydrol. Earth Syst. Sci.* **2013**, *17*, 2415–2434. [[CrossRef](#)]
36. Amjad, M.; Yilmaz, M.T.; Yucel, I.; Yilmaz, K.K. Performance evaluation of satellite-and model-based precipitation products over varying climate and complex topography. *J. Hydrol.* **2020**, *584*, 124707. [[CrossRef](#)]
37. Aggarwal, D.; Attada, R.; Shukla, K.K.; Chakraborty, R.; Kunchala, R.K. Monsoon precipitation characteristics and extreme precipitation events over Northwest India using Indian high resolution regional reanalysis. *Atmos. Res.* **2022**, *267*, 105993. [[CrossRef](#)]
38. Acharya, S.C.; Nathan, R.; Wang, Q.J.; Su, C.H.; Eizenberg, N. An evaluation of daily precipitation from a regional atmospheric reanalysis over Australia. *Hydrol. Earth Syst. Sci.* **2019**, *23*, 3387–3403. [[CrossRef](#)]
39. Bukovsky, M.S.; Karoly, D.J. A brief evaluation of precipitation from the North American Regional Reanalysis. *J. Hydrometeorol.* **2007**, *8*, 837–846. [[CrossRef](#)]
40. Gokmen, M. Spatio-temporal trends in the hydroclimate of Turkey for the last decades based on two reanalysis datasets. *Hydrol. Earth Syst. Sci.* **2016**, *20*, 3777–3788. [[CrossRef](#)]
41. Yazdandoost, F.; Moradian, S.; Izadi, A.; Bavani, A.M. A framework for developing a spatial high-resolution daily precipitation dataset over a data-sparse region. *Heliyon* **2020**, *6*, e05091. [[CrossRef](#)]
42. Li, X.; Chen, Y.; Wang, H.; Zhang, Y. Assessment of GPM IMERG and radar quantitative precipitation estimation (QPE) products using dense rain gauge observations in the Guangdong-Hong Kong-Macao Greater Bay Area, China. *Atmos. Res.* **2020**, *236*, 104834. [[CrossRef](#)]
43. Yu, Y.; Schneider, U.; Yang, S.; Becker, A.; Ren, Z. Evaluating the GPCC Full Data Daily Analysis Version 2018 through ETCCDI indices and comparison with station observations over mainland of China. *Theor. Appl. Climatol.* **2020**, *142*, 835–845. [[CrossRef](#)]
44. Tanır Kayıkçı, E.; Zengin Kazancı, S. Comparison of regression-based and combined versions of inverse distance weighted methods for spatial interpolation of daily mean temperature data. *Arab. J. Geosci.* **2016**, *9*, 690. [[CrossRef](#)]
45. Cavazos, T.; Hewitson, B.C. Performance of NCEP–NCAR reanalysis variables in statistical downscaling of daily precipitation. *Clim. Res.* **2005**, *28*, 95–107.
46. Xin, Y.; Lu, N.; Jiang, H.; Liu, Y.; Yao, L. Performance of ERA5 reanalysis precipitation products in the Guangdong-Hong Kong-Macao greater Bay Area, China. *J. Hydrol.* **2021**, *602*, 126791. [[CrossRef](#)]
47. Dhorde, A.G.; Zarenistanak, M. Three-way approach to test data homogeneity: An analysis of temperature and precipitation series over southwestern Islamic Republic of Iran. *J. Indian Geophys. Union* **2013**, *17*, 233–242.
48. Das, S.; Banerjee, S. Investigation of changes in seasonal streamflow and sediment load in the Subarnarekha-Burhabalang Basins using Mann-Kendall and Pettitt tests. *Arab. J. Geosci.* **2021**, *14*, 946. [[CrossRef](#)]
49. Fatichi, S.; Caporali, E. A comprehensive analysis of changes in precipitation regime in Tuscany. *Int. J. Climatol.* **2009**, *29*, 1883–1893. [[CrossRef](#)]
50. Rutkowska, A. Properties of the Cox–Stuart test for trend in application to hydrological series: The simulation study. *Commun. Stat.-Simul. Comput.* **2015**, *44*, 565–579. [[CrossRef](#)]
51. Militino, A.F.; Moradi, M.; Ugarte, M.D. On the performances of trend and change-point detection methods for remote sensing data. *Remote Sens.* **2020**, *12*, 1008. [[CrossRef](#)]
52. Salvacion, A.R.; Magcale-Macandog, D.B.; Cruz, P.C.S.; Saludes, R.B.; Pangga, I.B.; Cumagun, C.J.R. Evaluation and spatial downscaling of CRU TS precipitation data in the Philippines. *Model. Earth Syst. Environ.* **2018**, *4*, 891–898. [[CrossRef](#)]
53. Shi, H.; Li, T.; Wei, J. Evaluation of the Gridded CRU TS Precipitation Dataset with the Point Raingauge Records over the Three-River Headwaters Region. *J. Hydrol.* **2017**, *548*, 322–332. [[CrossRef](#)]
54. Jiang, Q.; Li, W.; Fan, Z.; He, X.; Sun, W.; Chen, S.; Wen, J.; Gao, J.; Wang, J. Evaluation of the ERA5 reanalysis precipitation dataset over Chinese Mainland. *J. Hydrol.* **2021**, *595*, 125660. [[CrossRef](#)]
55. Steinkopf, J.; Engelbrecht, F. Verification of ERA5 and ERA-Interim precipitation over Africa at intra-annual and interannual timescales. *Atmos. Res.* **2022**, *280*, 106427. [[CrossRef](#)]

56. Zhan, W.; Guan, K.; Sheffield, J.; Wood, E.F. Depiction of drought over sub-Saharan Africa using reanalyses precipitation data sets. *J. Geophys. Res. Atmos.* **2016**, *121*, 10–555. [[CrossRef](#)]
57. Assamnew, A.D.; Mengistu Tsidu, G. Assessing improvement in the fifth-generation ECMWF atmospheric reanalysis precipitation over East Africa. *Int. J. Climatol.* **2023**, *43*, 17–37. [[CrossRef](#)]
58. Akinsanola, A.A.; Ogunjobi, K.O.; Ajayi, V.O.; Adefisan, E.A.; Omotosho, J.A.; Sanogo, S. Comparison of five gridded precipitation products at climatological scales over West Africa. *Meteorol. Atmos. Phys.* **2017**, *129*, 669–689. [[CrossRef](#)]
59. Ongoma, V.; Chen, H. Temporal and spatial variability of temperature and precipitation over East Africa from 1951 to 2010. *Meteorol. Atmos. Phys.* **2017**, *129*, 131–144. [[CrossRef](#)]
60. Omoj, P.; Ogallo, L.; Oludhe, C.; Gitau, W. Temporal and spatial characteristics of the June-August seasonal rainfall and temperature over South Sudan. *J. Meteorol.* **2016**, *9*, 5. [[CrossRef](#)]
61. Hamadanel, M.; Zhu, Z.; Lu, R.; Shahid, S.; Ali, A.; Abdalla, I.; Elkanzi, M.; Bilal, M.; Bleiweiss, M.P. Spatio-temporal Investigations of Monsoon Precipitation and Its Historical and Future Trend over Sudan. *Earth Syst. Environ.* **2021**, *5*, 519–529. [[CrossRef](#)]

**Disclaimer/Publisher’s Note:** The statements, opinions and data contained in all publications are solely those of the individual author(s) and contributor(s) and not of MDPI and/or the editor(s). MDPI and/or the editor(s) disclaim responsibility for any injury to people or property resulting from any ideas, methods, instructions or products referred to in the content.